Ankyrin G restricts ion channel diffusion at the axonal initial segment before the establishment of the diffusion barrier

Anna Brachet,[1,2] Christophe Leterrier,[1,2] Marie Irondelle,[1,2] Marie-Pierre Fache,[1,2] Victor Racine,[3,4] Jean-Baptiste Sibarita,[3,5,6] Daniel Choquet,[5,6] and Bénédicte Dargent[1,2]

[1]Institut National de la Santé et de la Recherche Médicale, Unité Mixte de Rercherche 641, Marseille F-13916, France
[2]Université de la Méditerranée, Faculté de Médecine Secteur-Nord, Institut Fédératif de Recherche 11, Marseille F-13916, France
[3]Compartimentation et Dynamique Cellulaires, Institut Curie, Unité Mixte de Rercherche 144, Centre National de la Recherche Scientifique, 75248 Paris Cedex 05, France
[4]Institute of Molecular and Cell Biology, Proteos, Singapore 138673
[5]Centre National de la Recherche Scientifique, Unité Mixte de Rercherche 5091, Bordeaux F-33077, France
[6]Université de Bordeaux 2, Bordeaux F-33077, France

In mammalian neurons, the precise accumulation of sodium channels at the axonal initial segment (AIS) ensures action potential initiation. This accumulation precedes the immobilization of membrane proteins and lipids by a diffusion barrier at the AIS. Using single-particle tracking, we measured the mobility of a chimeric ion channel bearing the ankyrin-binding motif of the Nav1.2 sodium channel. We found that ankyrin G (ankG) limits membrane diffusion of ion channels when coexpressed in neuroblastoma cells. Site-directed mutants with decreased affinity for ankG exhibit increased diffusion speeds. In immature hippocampal neurons, we demonstrated that ion channel immobilization by ankG is regulated by protein kinase CK2 and occurs as soon as ankG accumulates at the AIS of elongating axons. Once the diffusion barrier is formed, ankG is still required to stabilize ion channels. In conclusion, our findings indicate that specific binding to ankG constitutes the initial step for Nav channel immobilization at the AIS membrane and precedes the establishment of the diffusion barrier.

Introduction

In mammalian neurons, the axonal initial segment (AIS) is a unique domain that plays a crucial role in the physiology of the nerve cell, as it orchestrates the interplay between electrogenesis and neuronal polarity. At the AIS, the concentration of voltage-gated ion channels ensures the generation of action potentials (Clark et al., 2009), whereas the peculiar nature of the AIS scaffold maintains the segregation between the axonal and somato-dendritic compartment for membrane constituents and for intracellular trafficking (Grubb and Burrone, 2010b).

At the molecular level, AIS functions require the segregation of the cytoskeletal adaptor ankyrin G (ankG; Salzer, 2003; Ogawa and Rasband, 2008). The ankG–βIV-spectrin scaffolding complex not only concentrates Nav1 sodium channels (Srinivasan et al., 1988; Zhou et al., 1998; Garrido et al., 2003; Lemaillet et al., 2003; Hedstrom et al., 2007) but also Kv7 potassium channels (Chung et al., 2006; Pan et al., 2006; Rasmussen et al., 2007) and cell adhesion molecules neurofascin-186 (NF-186) and neuronal cell adhesion molecule (NrCAM; Davis et al., 1996; Dzhashiashvili et al., 2007; Hedstrom et al., 2007). Importantly, the interaction between ankG and Nav1 channels is modulated by protein kinse CK2 (CK2) phosphorylation. CK2 concentrates at the AIS, phosphorylates the ankyrin-binding motif of Nav1 channels, and consequently regulates Nav1 interaction

The Rockefeller University Press $30.00
J. Cell Biol. Vol. 191 No. 2   383–395
www.jcb.org/cgi/doi/10.1083/jcb.201003042

JCB   **383**

with ankG (Bréchet et al., 2008). In addition, Kv1 voltage-gated potassium channels are concentrated at the distal AIS in certain types of neurons (Inda et al., 2006; Lorincz and Nusser, 2008).

A handful of studies have revealed that the functional organization of the AIS contributes to the establishment and the maintenance of neuronal polarity. Hedstrom et al. (2008) recently demonstrated that axons acquire the molecular characteristics of dendrites upon AIS disassembly, a result that was also confirmed in vivo (Sobotzik et al., 2009). This contribution occurs through intracellular and cell surface mechanisms, which are still poorly understood. Two studies have shown that the AIS acts as a cytoplasmic filter controlling the entry of vesicles in axons (Burack et al., 2000; Song et al., 2009). At the plasma membrane, the AIS forms a diffusion barrier that maintains the differences in protein and lipid composition between the somatodendritic and the axonal domain of neurons (Kobayashi et al., 1992; Nakada et al., 2003). Importantly, this fence restrains diffusion of axonal proteins independently of their ability to bind to ankG (Winckler et al., 1999; Boiko et al., 2007; Song et al., 2009). However, the mechanisms of the diffusion barrier and its assembly have yet to be determined.

The formation and the maintenance of the AIS depend on ankG expression (Zhou et al., 1998; Hedstrom et al., 2007), and in developing hippocampal neurons, its assembly occurs as soon as the axon starts elongating (stage 2–3 neurons; Boiko et al., 2007; Yang et al., 2007; Bréchet et al., 2008; Martin et al., 2008). Because the segregation of the AIS components appears before the general diffusion barrier (Nakada et al., 2003), this opens the possibility that ankG-dependent tethering is sufficient to restrain the surface diffusion of interacting proteins like Nav1 and adhesion protein. Therefore, the present study aims to analyze the precise role of ankG in the restriction of ion channel diffusion and the potential role of CK2 phosphorylation in this process in an attempt to unravel the mechanisms of the formation of a diffusion barrier at the AIS. We used a construct bearing the ankyrin-binding motif of Nav1.2, whose interaction with ankG is regulated by protein kinase CK2 phosphorylation (Bréchet et al., 2008). We were able to measure the surface diffusion of various Kv-Nav tetrameric ion channel constructs with different ankyrin binding properties. To do so, we used single-particle tracking (SPT; Borgdorff and Choquet, 2002; Tardin et al., 2003) with semiconductor quantum dot (QD) labeling (Dahan et al., 2003). Experiments in N2A cells demonstrated that ankG binding restricts the diffusion of chimeric ion channels and that phosphorylation of the ankyrin-binding motif by CK2 modulates this immobilization. In immature hippocampal neurons, ankG highly restricts the diffusion of ion channels in a CK2-dependent manner, as soon as it concentrates at the AIS. In mature neurons, ankG binding is still necessary for full immobilization, although the appearance of the diffusion barrier also slows the diffusion of proteins that do not bind ankG. Altogether, our findings strongly suggest that the immobilization of Nav1 is controlled by ankG from early stages. Such an immobilization occurs independently of the AIS diffusion barrier and may constitute the initial step toward its establishment.
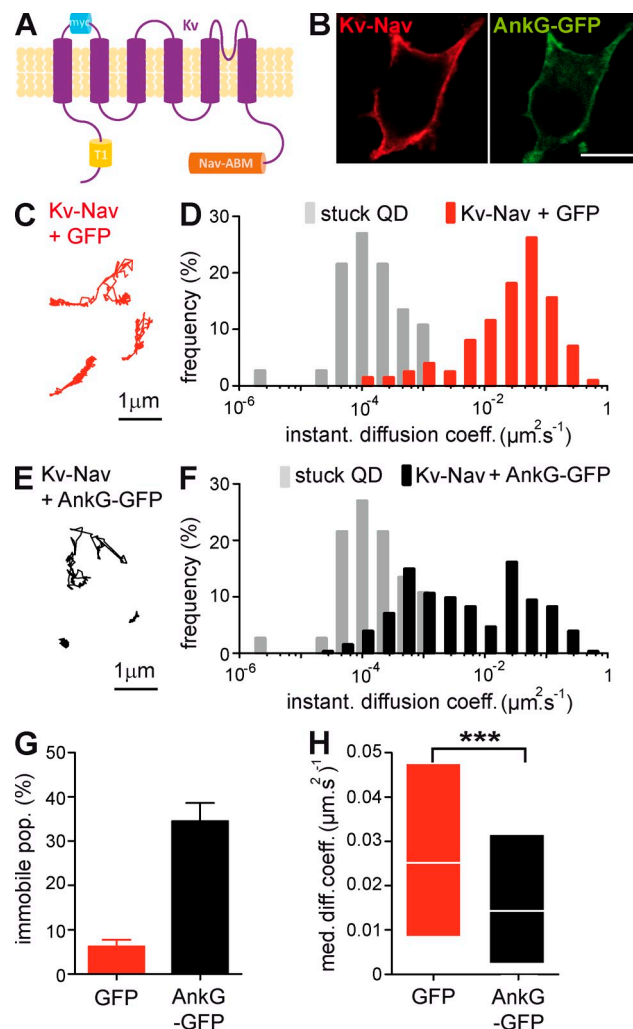

Figure 1. **ankG restricts Kv-Nav diffusion at the surface of N2A cells.** (A) Schematic representation of Kv-Nav chimera in which the C terminus of Kv2.1 was substituted by a segment encompassing the ankyrin-binding motif of Nav1.2. Note the presence of the tetramerization domain T1 in the N terminus of Kv2.1 and of an extracellular myc tag. (B) Surface expression of Kv-Nav in ankG-GFP–positive cells. Surface Kv-Nav was immunodetected with an antibody to myc (red), and ankG signal corresponds to the GFP fluorescent signal on fixed cells (green). Bar, 10 µm. (C and E) Representative examples of QD trajectories corresponding to Kv-Nav in GFP (red, C)- and ankG-GFP–expressing N2A cells (black, E). (D and F) DIDC of Kv-Nav in GFP (red, D)- and ankG-GFP–expressing N2A cells (black, F). The immobile population (D ≤ 0.00075 µm^2.s^{-1}) was defined from the DIDC of QDs stuck on the glass coverslips (gray). Trajectories for GFP (n = 198) and ankG-GFP (n = 253) conditions were analyzed from three and four independent experiments, respectively. (G) Histogram of the mean values ± SEM for the immobile population (percentage) of Kv-Nav in GFP and ankG-GFP conditions. (H) MDC (25–75% IQR) for the mobile population of Kv-Nav in GFP and ankG-GFP conditions. MW: ***, P < 0.001.

Results

ankG directly restrains ion channel diffusion when expressed in a neuronal cell line

To determine the effect of ankG on the surface diffusion of Nav1 channels, we first chose to heterologously express ankG and an ion channel chimera in neuroblastoma N2A cells. The C terminus of Kv2.1, which dictates its somatodendritic clustering (Lim et al., 2000), was deleted and replaced with the 1,080–1,203
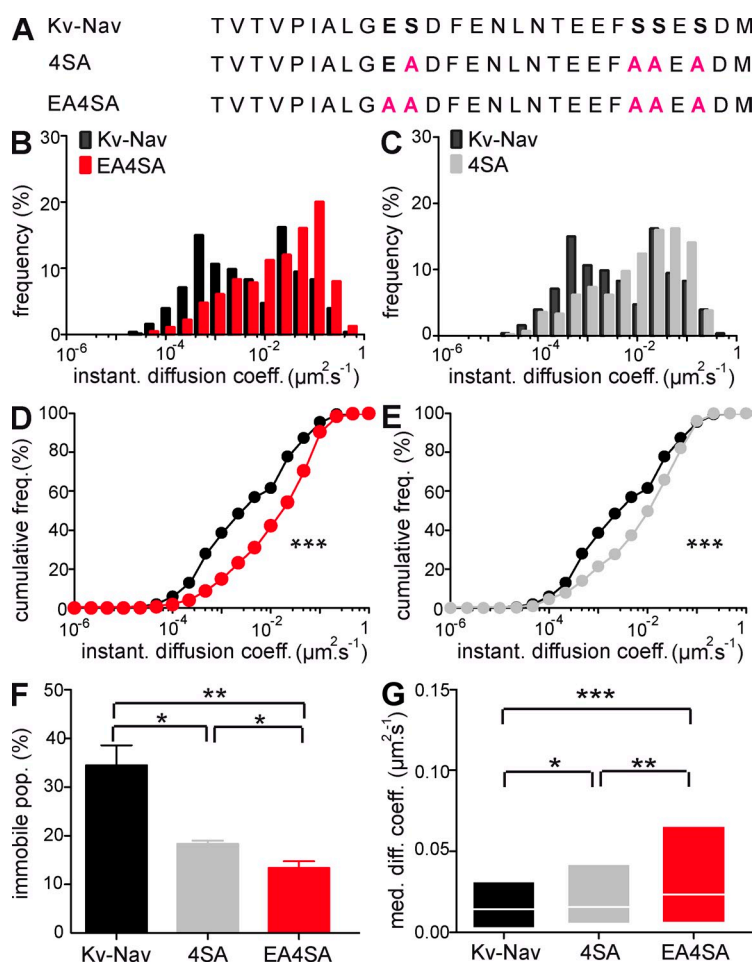
Figure 2. **Relationship between the binding capacities of site-directed Kv-Nav mutants with their restriction of diffusion in N2A cells.** (A) Sequence alignment of the ankyrin-binding domain for Kv-Nav, Kv-Nav 4SA (4SA), and Kv-Nav E4SA (E4SA) constructs. Critical residues for the interaction with ankG are represented in bold, and the mutated residues are highlighted in pink. (B–F) SPT of QD-labeled Kv-Nav with various ankyrin-binding affinities. (B and C) DIDC for EA4SA (red, B) and 4SA (gray, C). DIDC for Kv-Nav is represented in black for comparison. Trajectories for E4SA (n = 623) and 4SA (n = 419) conditions were analyzed from six and four independent experiments, respectively. (D and E) Cumulative frequencies of the instantaneous diffusion coefficients for Kv-Nav and 4SA (D) and Kv-Nav and E4SA (E). KS: ***, $P < 0.001$. (F) Histogram of the mean values ± SEM for the immobile population percentage of Kv-Nav, 4SA, and E4SA. MW: *, $P < 0.05$ and **, $P < 0.01$. (G) MDC (25–75% IQR) for the mobile population of Kv-Nav, 4SA, and E4SA. MW: *, $P < 0.05$; **, $P < 0.01$; and ***, $P < 0.001$.

segment of Nav1.2 that encompasses the ankyrin-binding motif (Kv2.1-Nav1.2, further called Kv-Nav; Fig. 1 A; Garrido et al., 2003; Bréchet et al., 2008). The resulting construct can tetramerize (Li et al., 1992), leading to a complex that has a membrane topology similar to Nav channels and bears four ankyrin-binding motifs. In N2A cells, expression of endogenous ankG was not detected by immunostaining (unpublished data). Kv-Nav was uniformly expressed at the plasma membrane in N2A cells (Fig. 1 B) in contrast to what is observed in human embryonic kidney cells in which Kv-Nav and ankG formed aggregates (Garrido et al., 2003), and transfected ankG-GFP displayed a homogenous submembrane localization (Fig. 1 B). This allowed us to analyze the effect of ankG on Kv-Nav mobility using an SPT method to measure surface diffusion (Borgdorff and Choquet, 2002; Tardin et al., 2003). Kv-Nav was coexpressed in N2A cells with either GFP or ankG-GFP, and surface channels were labeled on living cells with QDs using their myc extracellular tag. Rapid time-lapse imaging of individual QDs allowed us to analyze a large number of individual trajectories from which the distribution of the instantaneous diffusion coefficients (DIDC) could be determined. From the DIDC, we chose the maximum diffusion coefficient (D) of immobile QDs lying on the glass coverslip (D ≤ 0.00075 $\mu m^2.s^{-1}$) as the threshold, allowing us to define the immobile population (Fig. 1, D and F). Key mobility parameters such as median instantaneous diffusion coefficients (MDCs) and mean square displacement (MSD) could then be

extracted for the mobile particles (see Trajectory analysis in Materials and methods).

In cells expressing GFP, surface Kv-Nav was highly mobile, and the DIDC exhibited a broadly spread mobile population (Fig. 1, C and D). In ankG-GFP–expressing cells, the Kv-Nav trajectories were visually more restricted than the trajectories recorded in GFP-expressing cells (Fig. 1 E), and Kv-Nav DIDC was characterized by the appearance of a markedly less mobile population (Fig. 1 F). Compared with GFP, ankG-GFP expression strongly increased the population of immobile Kv-Nav, which rose from 6 ± 1 to 34 ± 4% (Fig. 1 G). The MDC of mobile particles significantly decreased between GFP and ankG-GFP conditions (0.025 $\mu m^2.s^{-1}$, interquartile range [IQR] of 0.0085/0.048 $\mu m^2.s^{-1}$, and 0.014 $\mu m^2.s^{-1}$, IQR of 0.0024/0.032 $\mu m^2.s^{-1}$, respectively; Mann and Whitney test [MW], $P < 0.0001$; Fig. 1 H). These data indicate that ankG restricts Kv-Nav diffusion in N2A cells.

Modulation of ankG binding affects the surface diffusion of ion channels

Neuronal sodium channels bind to ankG through their ankyrin-binding motif, which spans from amino acids 1,102 to 1,128 in the II–III intracellular loop for Nav1.2 (Garrido et al., 2003; Lemaillet et al., 2003). We recently showed that this interaction is regulated by CK2 phosphorylation (Bréchet et al., 2008). Nav1.2 and ankG associate with an apparent affinity constant (K_d) of $1.2 ± 0.4 × 10^{-6}$ and $0.9 ± 0.7 × 10^{-9}$ M before and after

CK2 phosphorylation, respectively (Bréchet et al., 2008). The mutation of the four serine residues (S1112, S1123, S1124, and S1126) to alanine (4SA mutant) in the Nav1.2 ankyrin binding site not only abolished the CK2-mediated affinity enhancement but also prevented the negative dominant effect of Kv-Nav on Nav accumulation at the AIS. Furthermore, these four serine mutations combined with the mutation of the glutamate residue E1111 (EA4SA mutant) fully abrogated the interaction of the Kv-Nav construct with ankG (Bréchet et al., 2008). Thus, these three structurally identical Kv-Nav constructs differing in their ankyrin-binding motif offer the unique opportunity to study the relationship between the strength of ankyrin binding and the surface mobility of ion channels (Fig. 2 A). It must be noted that these constructs are tetramers that bear four ankyrin-binding motifs, exacerbating their binding to ankG and its modulation in the different mutants. We measured the diffusion of site-directed Kv-Nav mutants in N2A cells expressing either GFP or ankG-GFP. In GFP cells, the immobile population of Kv-Nav, Kv-Nav 4SA, and Kv-Nav EA4SA were 6 ± 1, 7 ± 2, and $4 \pm 1\%$, respectively, with no significant difference between the three constructs (unpublished data). In ankG-GFP–expressing cells, the complete loss of ankG interaction (Kv-Nav EA4SA; Bréchet et al., 2008) induced a large shift of the DIDC toward higher values of diffusion coefficients and a significant difference in cumulative frequencies (Kolmogorov-Smirnov test [KS], $P < 0.0001$) when compared with Kv-Nav (Fig. 2, B and D). The immobile population decreased from 34 ± 4 to $13 \pm 1\%$ (MW, $P = 0.0095$; Fig. 2 F), and the MDC of the mobile population rose from $0.014 \ \mu m^2.s^{-1}$, IQR of $0.0024/0.032 \ \mu m^2.s^{-1}$, to $0.023 \ \mu m^2.s^{-1}$, IQR of $0.0059/0.066 \ \mu m^2.s^{-1}$, respectively (MW, $P < 0.0001$; Fig. 2 G). The diffusion behavior of the phospho-deficient Kv-Nav 4SA mutant (Bréchet et al., 2008) was also affected when compared with Kv-Nav (Fig. 2, C and E). The cumulative frequency of diffusion coefficients of Kv-Nav 4SA (Fig. 2 E) was significantly different from that of Kv-Nav and Kv-Nav EA4SA (KS, $P < 0.0001$ and $P = 0.001$, respectively) as well as the immobile population ($18 \pm 1\%$; MW, $P = 0.0286$ and $P = 0.0190$, respectively; Fig. 2 F) and the MDC of the mobile population ($0.016 \ \mu m^2.s^{-1}$, IQR of $0.0052/0.042 \ \mu m^2.s^{-1}$; MW, $P = 0.0242$ and $P = 0.0053$, respectively; Fig. 2 G). These findings indicate that site-directed mutants with decreasing affinities for ankG exhibited increasing diffusion speeds, highlighting the importance of ankG binding for chimeric ion channel immobilization at the plasma membrane.

ankG immobilizes ion channels at the nascent AIS of neurons

In the nervous system, the subcellular localization of ankG is highly specific, being segregated at the AIS and in the nodes of Ranvier (Kordeli et al., 1995). ankG accumulation also occurs at the AIS of developing hippocampal neurons maintained in vitro (Garrido et al., 2003; Boiko et al., 2007). In these cells, the AIS molecular assembly has already begun after day in vitro (DIV) 4 (Boiko et al., 2007; Yang et al., 2007; Bréchet et al., 2008; Martin et al., 2008), as visualized by the consistent immunostaining for ankG, Nav1, and NF-186 (Fig. 3 A). The AIS of cultured hippocampal neurons then develops a diffusion barrier that
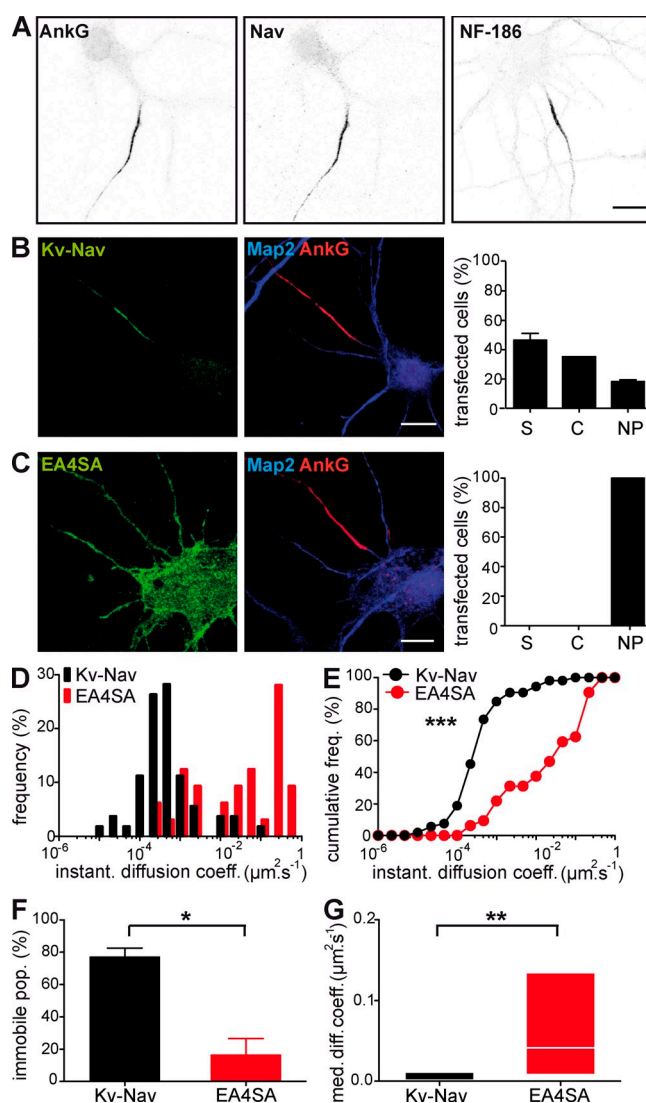

Figure 3. **Interaction with ankG restricts Kv-Nav diffusion at the AIS in young neurons.** (A) Accumulation of endogenous AIS components. DIV 4 hippocampal neurons were stained for ankG, Nav, and NF-186 (black). Bar, 10 µm. (B and C) Mutation of the ankyrin-binding motif perturbs polarized expression of surface Kv-Nav. Cell surface distribution of Kv-Nav (B) and Kv-Nav EA4SA (E4SA; C). DIV 4 cultured hippocampal neurons were transfected with the different constructs. Kv-Nav constructs were detected with an antibody against myc (green). The somatodendritic domain and the AIS were identified by MAP2 (blue) and ankG staining (red), respectively. Bars, 10 µm. (right) Histograms of the cell surface distribution for Kv-Nav (B) and EA4SA (C). The expression profiles of transfected (myc positive) neurons were classified into three categories: myc staining segregated at the AIS (segregated, S); distributed at the cell surface of the soma and proximal dendrites with a concentration at the AIS (concentrated, C); and uniformly distributed at the cell surface (nonpolarized, NP). 100% represents the total population of transfected neurons. Data are means ± SEM with $n = 165$ and 52 from four and two independent experiments for Kv-Nav and EA4SA, respectively. (D and E) Distribution (D) and cumulative frequency (E) of the instantaneous diffusion coefficients of Kv-Nav and EA4SA ($n = 53$ and 32 trajectories from four independent experiments for Kv-Nav and EA4SA, respectively). KS: ***, $P < 0.001$. (F) Histogram of the mean values ± SEM for the immobile population of Kv-Nav and EA4SA. MW: *, $P < 0.05$. (G) MDC (25–75% IQR) of the mobile population of Kv-Nav and EA4SA. MW: **, $P < 0.01$.

restricts the mobility of membrane proteins and phospholipids, but this general diffusion barrier is not yet formed in DIV 4 hippocampal neurons (Nakada et al., 2003; Boiko et al., 2007).
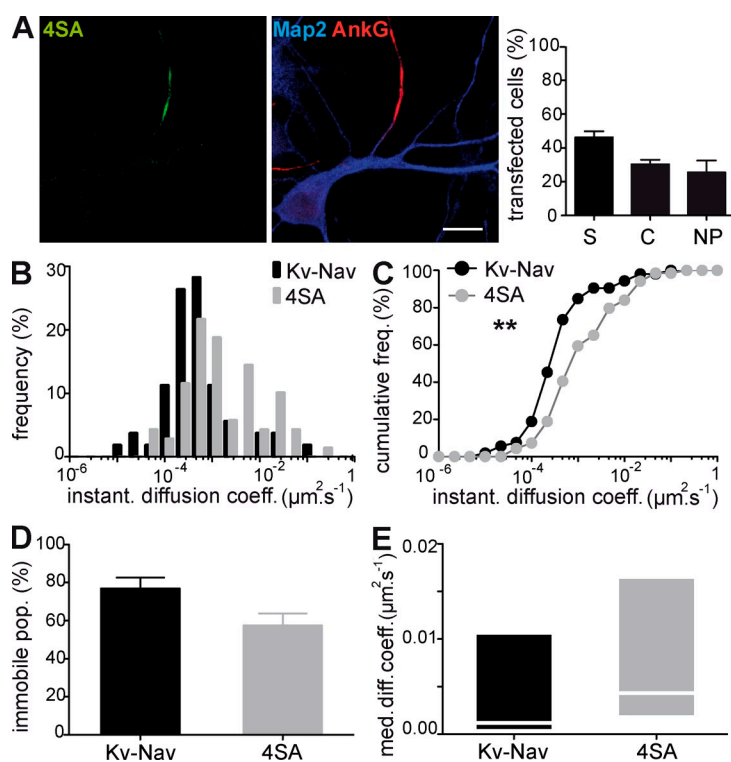
Figure 4. **Involvement of the ankyrin-binding motif serine residues in Kv-Nav immobilization at the AIS in young neurons.** (A) Cell surface distribution of Kv-Nav 4SA (4SA), a phosphodeficient mutant, in DIV 4 hippocampal neurons. Quantification of the cell surface distribution of 4SA is represented on the right and was performed as described in Fig. 3. Data are means ± SEM with $n = 144$ from four different experiments. Bar, 10 µm. (B and C) Distributions (B) and cumulative frequencies (C) of the instantaneous diffusion coefficients of 4SA ($n = 69$ trajectories from five independent experiments for 4SA. KS: **, $P < 0.01$). (D) Histogram of the mean values ± SEM for the immobile population of Kv-Nav and Kv-Nav 4SA. (E) MDC (25–75% IQR) of the mobile population of Kv-Nav and Kv-Nav 4SA.

We took advantage of these observations to assess the specific role of ankG in ion channel diffusion. We first examined the surface distribution of Kv-Nav and Kv-Nav EA4SA when they were expressed in DIV 4 neurons (Fig. 3, B and C). Kv-Nav was highly concentrated at the AIS of 81.5% of the expressing cells, whereas Kv-Nav EA4SA was not polarized in any of the counted neurons. These observations are in line with our previous studies in more mature cells (i.e., DIV 10 neurons; Garrido et al., 2003; Bréchet et al., 2008). We next compared Kv-Nav and Kv-Nav EA4SA mobility using ankG-GFP for AIS identification (Fig. 3, D–G). A large fraction (77 ± 6%) of the Kv-Nav population was immobile at the AIS (Fig. 3 F). This restriction relies on the ability of Kv-Nav to bind to ankG, as DIDC and the cumulative frequency of Kv-Nav EA4S4A shifted to higher diffusion coefficients (KS, $P < 0.0001$; Fig. 3, D and E). As a result, only 16 ± 10% of the Kv-Nav EA4SA population was immobile at the AIS (MW, $P = 0.0294$; Fig. 3 F), and the mobile population diffused more than the Kv-Nav population (0.0015 µm².s⁻¹, IQR of 0.0010/0.011 µm².s⁻¹, for Kv-Nav and 0.0413 µm².s⁻¹, IQR of 0.0082/0.13 µm².s⁻¹, for Kv-Nav EA4SA; MW, $P = 0.0019$; Fig. 3 G). We verified that the accumulation of endogenous ankG was sufficient to account for the drastic reduction of Kv-Nav mobility by substituting NrCAM-GFP for ankG-GFP to visualize the AIS (Fig. S1). In this condition, the immobile population was 78 ± 8% for Kv-Nav compared with 27 ± 2% for Kv-Nav EA4SA, and the MDC of the mobile population was 0.0019 µm².s⁻¹ for Kv-Nav versus 0.071 µm².s⁻¹ for Kv-Nav EA4SA (IQR of 0.0011/0.0070 and 0.021/0.12 µm².s⁻¹, respectively; MW, $P = 0.0009$; Fig. S1). These results show that the specific interaction with ankG dampens the diffusion of Kv-Nav in young hippocampal neurons. Thus, the nascent accumulation of ankG is sufficient to markedly and specifically immobilize ankyrin-binding ion channels in developing neurons.

CK2 phosphorylation modulates ion channel diffusion at the nascent AIS in young neurons

We next examined how modulation of ankG binding properties impacts the surface mobility of ion channels in young neurons. Kv-Nav 4SA, which binds ankG with a reduced affinity, still concentrates at the AIS of DIV 4 neurons (Fig. 4 A), similar to what was observed in DIV 10 neurons (Bréchet et al., 2008). However, the diffusion properties of Kv-Nav 4SA were significantly different from those of Kv-Nav, as a shift toward higher diffusion coefficients was seen in the DIDC and in the cumulative frequency (KS, $P = 0.002$; Fig. 4, B and C). It should be noted that the significant enhancement of mobility observed in the cumulative frequency of diffusion coefficients was not associated with a significant change of the immobile population (77 ± 6% for Kv-Nav and 57 ± 6% for Kv-Nav 4SA; Fig. 4 D) nor in the MDC of the mobile population (0.0015 µm².s⁻¹, IQR of 0.0010/0.011 µm².s⁻¹, for Kv-Nav and 0.0043 µm².s⁻¹, IQR of 0.0018/0.016 µm².s⁻¹, for Kv-Nav 4SA; Fig. 4 E). These results indicate that the mutation of CK2-targeted serines alters Kv-Nav immobilization in young neurons. To further assess the role of CK2 phosphorylation on Kv-Nav immobilization, we analyzed Kv-Nav diffusion upon acute inhibition of CK2 activity using DMAT (2-dimethylamino-4,5,6,7-tetrabromo1 H-benzimidazole), a potent CK2 inhibitor (Pagano et al., 2004). Kv-Nav diffusion was first measured in control medium (vehicle condition; t = 0 min; Fig. 5 A). After replacement of the medium with an equivalent solution supplemented with DMAT, the movements of the same QD-labeled ion channels were then repeatedly recorded for a further 10–25 min. The mean diffusion coefficients were calculated for this period (t = 10–25 min; Fig. 5 A) and compared with the initial coefficients. After 10–25 min of DMAT application, the MDC

of initially immobile QDs increased significantly (from 0.00027 $\mu m^2.s^{-1}$, IQR of 0.00013/0.00043 $\mu m^2.s^{-1}$, to 0.00060 $\mu m^2.s^{-1}$, IQR of 0.00027/0.0029 $\mu m^2.s^{-1}$; Wilcoxon signed rank test [WSR], P = 0.0004; Fig. 5 A). This was not observed in control cells treated with vehicle instead of DMAT (from 0.00023 $\mu m^2.s^{-1}$, IQR of 0.000098/0.00040 $\mu m^2.s^{-1}$, to 0.00018 $\mu m^2.s^{-1}$, IQR of 0.000091/0.00056 $\mu m^2.s^{-1}$; Fig. 5 B). We next examined the effect of DMAT on the diffusion of the phosphodeficient mutant Kv-Nav 4SA. No significant difference was measured in the MDC before and after 10–25 min of either DMAT or vehicle applications (from 0.00020 $\mu m^2.s^{-1}$, IQR of 0.00010/0.00025 $\mu m^2.s^{-1}$, to 0.00023 $\mu m^2.s^{-1}$, IQR of 0.00017/0.00041 $\mu m^2.s^{-1}$, for DMAT and from 0.00022 $\mu m^2.s^{-1}$, IQR of 0.000086/0.00047 $\mu m^2.s^{-1}$, to 0.00031 $\mu m^2.s^{-1}$, IQR of 0.00024/0.00050 $\mu m^2.s^{-1}$, for vehicle; Fig. 5, C and D). Comparison across conditions between DMAT and vehicle treatments indicated different MDCs for Kv-Nav, but not for Kv-Nav 4SA (MW for Kv-Nav, P = 0.0078; Fig. 5, C and D). Altogether, these data strongly suggest that inhibition of CK2 phosphorylation is able to alter Kv-Nav mobility at the AIS.

We next examined whether the increase in mobility induced by CK2 inhibition could later destabilize the concentration of ankyrin-binding ion channels at the AIS. We quantified the immunostaining of ankG and endogenous Nav1 channels in neurons treated for 4, 8, or 24 h with either DMAT or vehicle. The inhibition of CK2 activity induced a progressive decrease in Nav1 labeling at the AIS (80 ± 5% of control value after 4 h, 77 ± 7% after 8 h, and 69 ± 6% after 24 h), a process that seems to occur before perturbation of ankG concentration (decreasing to 86 ± 55% after 4 h, 86 ± 6% after 8 h, and 48 ± 4% after 24 h; Fig. 5 E). Collectively, these results show that binding affinity, restriction of diffusion, and AIS concentration are correlated in young neurons. They also demonstrate that CK2 can modulate Kv-Nav binding to ankyrin and Kv-Nav immobilization in the nascent AIS.

ankG restricts ion channel diffusion at the AIS of mature neurons

We then studied the relationship between ankG binding and the restriction of ion channel diffusion in mature neurons, which develop a general diffusion barrier at the AIS (Winckler et al., 1999; Nakada et al., 2003). To discriminate between an effect driven by direct ankG binding from the effect of the general diffusion barrier, we compared the diffusion behaviors of Kv-Nav, Kv-Nav 4SA, and Kv-Nav EA4SA in DIV 10 neurons. A loss of compartmentalization was observed for Kv-Nav EA4SA, but not for Kv-Nav 4SA (Fig. 6 A), in agreement with our previous study (Bréchet et al., 2008). In DIV 10 neurons, the diffusion properties of Kv-Nav EA4SA were different when compared with Kv-Nav (Fig. 6 B): the DIDC and the cumulative frequency of diffusion coefficients shifted toward higher values for Kv-Nav EA4SA (KS, P < 0.0001), and the percentage of the immobile population dropped to 43 ± 3% (MW, P = 0.012; Fig. 6 C). Note that the MDC of the Kv-Nav EA4SA mobile population was not significantly different from that of Kv-Nav (0.0075 $\mu m^2.s^{-1}$, IQR of 0.0018/0.017 $\mu m^2.s^{-1}$; Fig. 6 D). In comparison, Kv-Nav and Kv-Nav 4SA displayed similar diffusion properties (Fig. 6, B and C): we did not find any significant differences in the DIDC, the cumulative frequency of diffusion coefficients (Fig. 6, B and C), the immobile population
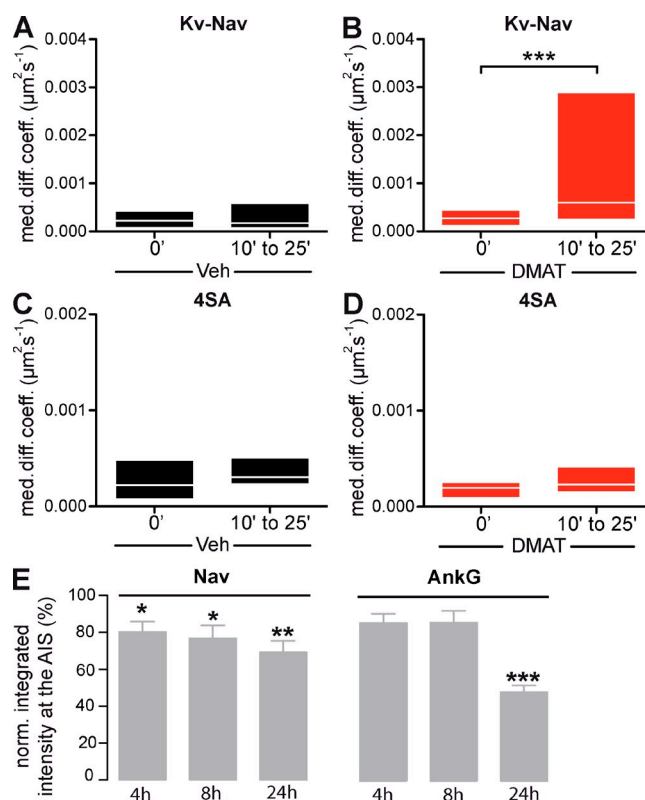

Figure 5. **Pharmacological inhibition of CK2 releases ion channels from immobility and destabilizes ion channel concentration at the AIS in young neurons.** (A–D) SPT on Kv-Nav (A and B) and Kv-Nav 4SA (C and D) in DIV 4 neurons in the presence of the CK2 inhibitor DMAT. QD trajectories were recorded at the AIS of DIV 4 neurons acutely treated with 50 µM DMAT or a vehicle only during the indicated time intervals. For Kv-Nav, trajectories for vehicle (n = 14) and DMAT (n = 19) were analyzed from three and four independent experiments, respectively. For Kv-Nav 4SA, trajectories for vehicle (n = 11) and DMAT (n = 12) were analyzed from three indepent experiments. MDC (25–75% IQR) before and after drug addition for Kv-Nav (A and B) and Kv-Nav 4SA (C and D). WSR: ***, P < 0.001. (E) Effect of DMAT on the accumulation of AIS components in young neurons. DIV 3 cells were treated with either 50 µM DMAT or with DMSO (control cells) for 4, 8, and 24 h and were subsequently immunostained for Nav1 channels and ankG. Quantification of the respective fluorescence intensity was achieved and was normalized to 100%, representing the staining intensity measured in control cells. Histogram represents the normalized mean values ± SEM. The number of quantified AISs range from 69 to 118 per condition (two independent experiments). t test: *, P < 0.05; **, P < 0.01; and ***, P < 0.001.

(78 ± 4% for Kv-Nav and 72 ± 8% for Kv-Nav 4SA), and the MDC of the mobile population (0.0028 $\mu m^2.s^{-1}$ for Kv-Nav and 0.0074 $\mu m^2.s^{-1}$ for Kv-Nav 4SA; IQR of 0.0019/0.012 and 0.0017/0.021 $\mu m^2.s^{-1}$, respectively; Fig. 6, B and C). These observations suggested that CK2 modulation of Kv-Nav mobility might be occluded in DIV 10 neurons in contrast to what was observed in DIV 4 neurons (Figs. 4 and 5). Therefore, we analyzed Kv-Nav diffusion upon acute inhibition of CK2 activity in a similar manner as described for young neurons (Fig. 5). From 10 to 20 min after drug application, the MDC of initially immobilized channels varied significantly in DMAT but not in vehicle conditions (from 0.00013 $\mu m^2.s^{-1}$, IQR of 0.000080/0.00022 $\mu m^2.s^{-1}$, to 0.00020 $\mu m^2.s^{-1}$, IQR of 0.00012/0.00085 $\mu m^2.s^{-1}$, for DMAT; WSR, P = 0.0186; and from 0.00016 $\mu m^2.s^{-1}$, IQR of 0.000072/0.00039 $\mu m^2.s^{-1}$, to 0.00026 $\mu m^2.s^{-1}$, IQR of
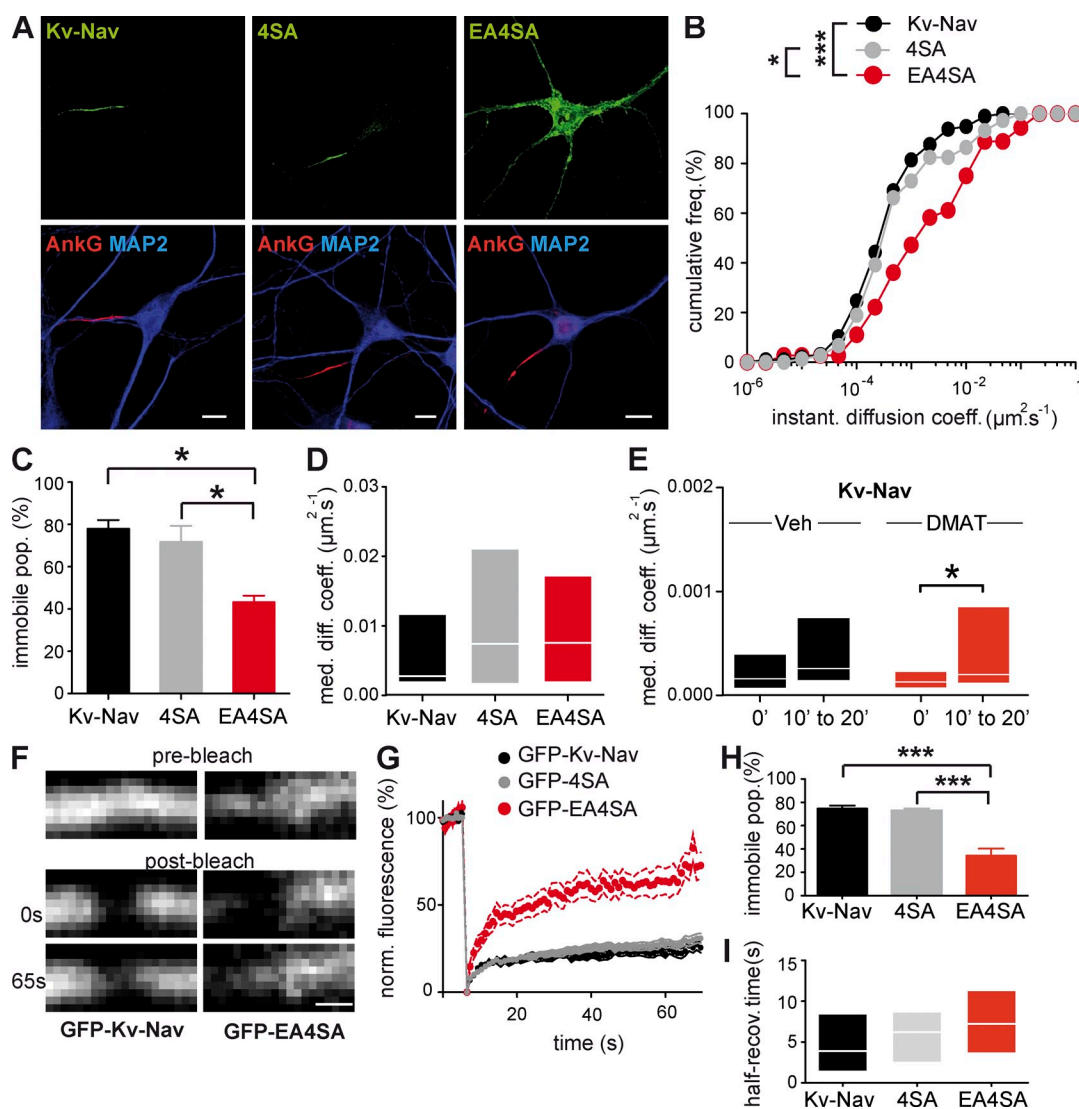
Figure 6. **Interaction with ankG restricts Kv-Nav diffusion at the AIS of mature neurons.** (A) Surface distribution of Kv-Nav, Kv-Nav 4SA (4SA), and Kv-Nav EA4SA (EA4SA) in DIV 10 hippocampal neurons. Cultured hippocampal neurons were transfected with the indicated constructs. Kv-Nav and mutants were detected, and neurons were stained as explained in Fig. 3. Bars, 10 µm. (B–E) SPT of QD-labeled Kv-Nav and mutants in DIV 10 neurons. (B) Cumulative frequencies of the instantaneous diffusion coefficients of Kv-Nav, 4SA, and EA4SA. Trajectories for Kv-Nav ($n = 97$), 4SA ($n = 75$), and EA4SA ($n = 36$) were analyzed from six, five, and five independent experiments, respectively. KS: *, $P < 0.05$ and ***, $P < 0.001$. (C) Histogram of the mean values ± SEM for the immobile population percentage of Kv-Nav, 4SA, and EA4SA. MW: *, $P < 0.05$. (D) MDC (25–75% IQR) of the mobile population of Kv-Nav, 4SA, and EA4SA. (E) SPT on Kv-Nav at the AIS of DIV 10 neurons acutely treated with 50 µM DMAT or vehicle. MDC (25–75% IQR) before and after drug addition. Analysis was performed as explained in Fig. 5. For DMAT condition, $n = 11$ trajectories from four independent experiments. For vehicle condition, $n = 10$ trajectories from three independent experiments. WSR: *, $P < 0.05$. (F–I) Analysis of the diffusion properties of GFP–Kv-Nav and mutants in DIV 10 neurons by FRAP. $n = 22$, 27, and 17 bleached regions that were analyzed from three independent experiments for Kv-Nav, EA4SA, and 4SA, respectively. (F) Representative examples of GFP–Kv-Nav (left) and GFP-EA4S4A (right) fluorescence at the AIS before photobleaching, immediately after photobleaching, and 65 s later. Bar, 1 µm. (G) Plot of the normalized mean fluorescence intensity ± SEM for GFP–Kv-Nav and mutants versus time before and after photobleaching. (H) Histogram of the mean values ± SEM for the immobile population percentage of indicated constructs. MW: ***, $P < 0.001$. (I) Histogram of the median values ± IQR (25–75%) for the half-recovery time constant of indicated constructs.

$0.00015/0.00074 \, \mu m^2.s^{-1}$, for vehicle; Fig. 6 E). However, comparison across DMAT and vehicle conditions, implying the use of unpaired statistical tests, showed no significant difference (Fig. 6 E). Altogether, these data show that Kv-Nav immobilization still depends on ankG binding in mature neurons but that the CK2 modulation of Kv-Nav mobility is largely attenuated at this stage.

We next conducted experiments using FRAP (Bats et al., 2007) to compare the fluorescence recovery of GFP–Kv-Nav, GFP–Kv-Nav 4SA, and GFP–Kv-Nav EA4SA in DIV 10

neurons (Fig. 6, F–I). NrCAM-mCherry coexpression was used to visualize the AIS. The percentage of the immobile population of GFP–Kv-Nav 4SA and of GFP–Kv-Nav was higher than that of GFP–Kv-Nav EA4SA (71 ± 2, 75 ± 2, and 32 ± 6%, respectively; MW, $P < 0.0001$ for both pairs; Fig. 6 H). The half-recovery time of the three constructs was in the same range of magnitude and did not differ significantly (Fig. 6 I). This independent measurement of Kv-Nav mobility confirms that, in mature neurons, a direct interaction with ankG restricts diffusion of ion channels.

Figure 7. **The diffusion barrier is formed in DIV 10 but not in DIV 4 neurons.** Comparison of the diffusion behavior of a mutant deficient for ankyrin binding (Kv-Nav EA4SA) at two development stages, DIV 4 (A–C) and DIV 10 (D–F), and in two distinct compartments of the plasma membrane, the AIS and proximal dendrites. For DIV 4, $n = 18$ and 20 trajectories from three and two independent experiments at the AIS and at proximal dendrites, respectively. For DIV 10, $n = 36$ and 41 trajectories from three and two independent experiments at the AIS and at proximal dendrites, respectively. (A and D) Cumulative frequencies of the instantaneous diffusion coefficients at the AIS and in proximal dendrites in DIV 4 (A) and DIV 10 (D) neurons. KS: ***, $P < 0.001$. (B and E) Histogram of the mean values ± SEM of the immobile population percentage in DIV 4 (B) and DIV 10 (E) neurons at the AIS and in proximal dendrites. MW: *, $P < 0.05$. (C and F) MDC (25–75% IQR) of the mobile population at the AIS and in proximal dendrites. MW: **, $P < 0.01$. (G) Mean plot of the MSD of the mobile population versus time (solid line) ± SEM (dotted line) for the indicated period for the mobile population at the AIS of DIV 4 and DIV 10 neurons. (H) Magnification of the boxed area in G.
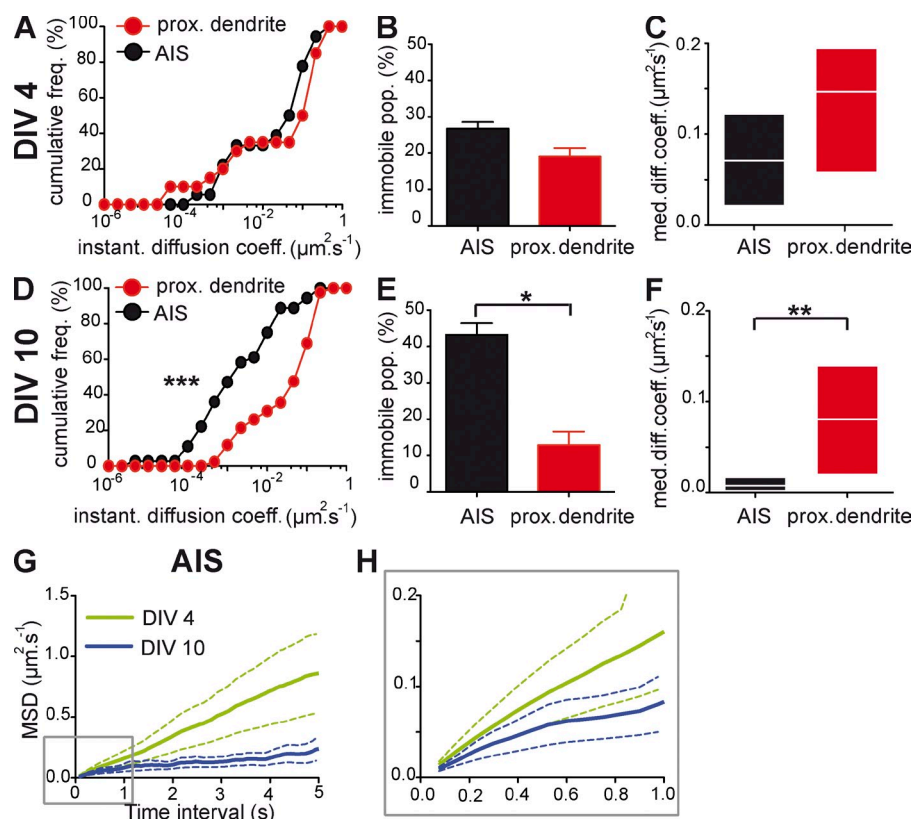
A diffusion barrier restrains the diffusion of an ion channel deficient for ankyrin binding in mature neurons

The differential effect of CK2 on Kv-Nav immobilization at the AIS between young and mature neurons may be linked to the appearance of the diffusion barrier between these stages (Winckler et al., 1999; Nakada et al., 2003). If this additional mechanism is functional in DIV 10 neurons, the diffusion behavior of Kv-Nav EA4SA should be different in proximal dendrites and in the AIS. To test this hypothesis, we compared the diffusion properties of Kv-Nav EA4SA in DIV 4 and DIV 10 neurons using NrCAM-GFP for the assignment of AIS and proximal dendrite. In DIV 4 neurons, Kv-Nav EA4SA diffusion properties were identical in the AIS and the proximal dendrites (Fig. 7, A–C). In DIV 10 neurons, the cumulative frequencies of the diffusion coefficients were significantly different (KS, $P < 0.0001$; Fig. 7 D). The percentages of the immobile populations were 13 ± 4% for proximal dendrites and 43 ± 3% for the AIS (MW, $P = 0.0358$; Fig. 7 E), and the mobile fraction diffused faster in proximal dendrites ($0.080 \ \mu m^2.s^{-1}$, IQR of $0.020/0.14 \ \mu m^2.s^{-1}$) than at the AIS ($0.0075 \ \mu m^2.s^{-1}$, IQR of $0.0018/0.017 \ \mu m^2.s^{-1}$; MW, $P = 0.0014$; Fig. 7 F). We further analyzed the confinement properties of the mobile population at the AIS by evaluating its MSD. In DIV 4 neurons, the MSD of Kv-Nav EA4SA increased linearly as a function of time, indicating a free diffusing pattern of surface diffusion. In DIV 10 neurons, MSD plotted as a function of time was negatively curved, demonstrating that the protein moved in a confined space (Fig. 7, G and H). To exclude the possibility that the differences observed were caused by a low level of ankG expression in DIV 4 cells, we replaced NrCAM-GFP by ankG-GFP

as an AIS marker (Fig. S2). In this condition, Kv-Nav EA4SA diffusion properties were similar for proximal dendrites and for the AIS, similar to what was observed in the presence of NrCAM-GFP (Fig. 7, A–C). These data show that an ion channel deficient for ankG binding exhibited a restricted mobility at the AIS of mature neurons, but not of immature neurons. This is likely to result from the appearance of a general diffusion barrier, in line with previous studies (Winckler et al., 1999; Nakada et al., 2003). Altogether, these findings revealed that a two-step mechanism of diffusion restriction takes place at the AIS. As soon as the scaffold protein concentrates at the AIS, before the assembly of the diffusion barrier (DIV 4), a tight and CK2-regulated binding to ankG is required to immobilize Nav channels. Once the barrier is formed (DIV 10), ion channel immobilization still requires ankG binding, but the presence of the barrier also immobilizes proteins that bind weakly or do not bind ankG.

Discussion

In the present study, we show that ankG restricts diffusion of Kv-Nav chimeric ion channels through interaction with the Nav1.2 ankyrin-binding motif in N2A cells and hippocampal neurons. In young neurons, CK2 is able to modulate the immobilization of Kv-Nav. In mature neurons, ankG is still necessary for Kv-Nav immobilization, and CK2 modulation is attenuated. Our findings demonstrate that a CK2-regulated binding to ankyrin is initially required to immobilize Nav channels at the AIS before the assembly of the diffusion barrier. Once formed, the diffusion barrier can partially supplement the role of ankG in immobilizing ion channels, as demonstrated with Kv-Nav mutants

with reduced ankyrin binding. Thus, early immobilization of ankyrin-binding proteins may constitute a preliminary step in the formation of the diffusion barrier (Winckler et al., 1999; Nakada et al., 2003).

Diffusion of ankyrin-binding proteins at the AIS

SPT with QDs was first used to study diffusion of the glycine receptor in spinal cord neurons (Dahan et al., 2003). The main benefit of this technique is that it allows the investigator to obtain a detailed DIDC rather than a mean coefficient of diffusion-like ensemble methods such as FRAP (Triller and Choquet, 2008). The diffusion coefficient values obtained for Kv-Nav constructs are in the order of $D = \sim0.001 \ \mu m^2.s^{-1}$ in both young and mature neurons. Compared with other membrane proteins, this places AIS channels at the slowest part of the diffusion spectrum (for review see Groc and Choquet, 2008). Early results suggested a slow diffusion of Nav1 channels at the axon hillock ($D = \sim0.015 \ \mu m^2.s^{-1}$; Angelides et al., 1988), later confirmed by SPT of toxin-tagged channels ($D = \sim0.01 \ \mu m^2.s^{-1}$; Nakada et al., 2003). For adhesion proteins, a diminished diffusion of neurofascin at the AIS was observed using bound latex beads ($D = \sim0.01 \ \mu m^2.s^{-1}$; Winckler et al., 1999; Boiko et al., 2007). The slower diffusion observed in the present study could be caused by the higher sensitivity of the SPT/QD method. Alternatively, immobilization could be enhanced by the tetrameric nature of Kv-Nav constructs that bear four ankyrin-binding motifs. The tetravalence of Kv-Nav complexes is likely to exacerbate the differences in the ankyrin binding properties of Kv-Nav and its mutants and could have helped to discriminate their differences in diffusive properties. Nevertheless, one of the main goals of future studies will be to measure the diffusive properties of endogenous Nav channels that bear a single ankyrin-binding motif.

Diffusion-trapping model for accumulation of ankyrin-binding proteins at the AIS

Studies of chimeras containing different portions of the Nav1.2 sodium channel have shown that these constructs are sent to both somatodendritic and axonal compartments before being selectively endocytosed (Fache et al., 2004) and retained at the AIS because of their interaction with ankG via the ankyrin-binding motif (Garrido et al., 2003; Lemaillet et al., 2003). By using N2A cells and neurons at different stages of development, we now show that the slow diffusion of Kv-Nav depends on its binding to ankyrin. Downstream of targeting mechanisms, this supports a diffusion-trapping mechanism for ankyrin-binding channels at the AIS. Trapping of ion channels and adhesion proteins by ankG could explain how they progressively concentrate at the AIS in developing neurons (Xu and Shrager, 2005; Boiko et al., 2007; Hedstrom et al., 2007). Interestingly, the ankG–Nav1 interaction is regulated by CK2 phosphorylation, and the restriction of CK2 to the AIS can explain why Nav1 channels are preferentially trapped by ankG at the AIS rather than by ankB further down the axon (Bréchet et al., 2008). Ankyrin-based trapping of L1CAM by ankB has been demonstrated in axonal growth cones (Gil et al., 2003) and is also dependent on

phosphorylation by an unknown kinase (Garver et al., 1997). Here, perturbing ankG–Nav1 interactions by inhibiting CK2 with the DMAT inhibitor affects ion channel diffusion and accumulation at the AIS. CK2 inhibition leads to an enhanced diffusion of Kv-Nav after 10 min and to a decrease in endogenous Nav1 concentration at the AIS after 4–8 h. The difference between the short-term effect on diffusion and the long-term effect on localization could seem paradoxical. However, differences in diffusion can be very slow to affect steady-state localization of membrane proteins, as shown by mathematical modeling of neurotransmitter receptors at the postsynaptic density (Holcman and Triller, 2006; Sekimoto and Triller, 2009).

Primary role of ankG in restricting diffusion at the AIS

The primary role of ankG in AIS assembly and maintenance is now established (Zhou et al., 1998; Hedstrom et al., 2007, 2008), but its role in the diffusion barrier has not been clearly addressed yet (Lasiecka et al., 2008). Previous studies have shown that there is a correlation between ankyrin concentration at the AIS and the restriction of the diffusion of neurofascin (Boiko et al., 2007) and lipids in older neurons (Nakada et al., 2003). In a recent study, knocking down ankG expression allowed VAMP2 to diffuse more freely at the AIS of young neurons (Song et al., 2009). First, ankG is able to specifically restrict the diffusion of ankG-binding constructs before the diffusion barrier appears. Second, after the diffusion barrier has established at DIV 10, all constructs are slowed at the AIS compared with proximal dendrites, but constructs that bind to ankG are more immobile than constructs that do not. We could separate the immobilization of ankyrin-binding proteins from the general immobilization of membrane proteins caused by the diffusion barrier because, in our system, we observed a concentration of ankG at the AIS by DIV 4, similar to other studies (Hedstrom et al., 2007; Song et al., 2009), before seeing an effect of the diffusion barrier that is present at DIV 10. An interesting question, given the large spread of DIDC for Kv-Nav, is the relative contribution of ankG mobility, as scaffolding complexes have been shown to be dynamic (Specht and Triller, 2008). However, the mobility of such scaffolds is usually very low compared with the diffusion of membrane proteins. The DIDC spread is more likely caused by rapid association–dissociation events with ankG along the trajectories, resulting in a diminished diffusion coefficient.

Subsequent steps in the diffusion barrier assembly

Our results show that ankyrin-binding proteins are immobilized at the AIS as soon as DIV 4, whereas the mobility of ankyrin-noninteracting proteins was restricted at a later stage of development. This suggests that immobilization of ankyrin-binding proteins is a preliminary step in the assembly of the diffusion barrier. In the "fence and pickets" model of the AIS diffusion barrier (Nakada et al., 2003), ankG acts as a fence post to recruit ankyrin-binding membrane proteins as pickets. If ankyrin-binding pickets are sufficient to slow down all AIS membrane proteins, overexpressing NrCAM-GFP pickets at the AIS of

DIV 4 neurons should have a significant effect on the diffusion of Kv-Nav E4SA, which does not interact with ankG. However, we observed that NrCAM-GFP only slightly decreased Kv-Nav E4SA diffusion (Fig. 6). This could be because overexpression of NrCAM-GFP is not sufficient to reach a critical concentration of pickets (Nakada et al., 2003) or NrCAM-GFP is not as functional as endogenous NrCAM, as it lacks the extracellular FnIII domain that was swapped for GFP (Falk et al., 2004). More likely, the presence of more membrane ankyrin-binding proteins is not sufficient to create a diffusion barrier. The AIS still develops and matures between DIV 4 and DIV 10, with the assembly of additional components. βIV-Spectrin (Berghs et al., 2000) is likely to be another constituent of the fence, although its depletion affects the diffusion of only L1CAM along the AIS (Nishimura et al., 2007). Specific lipids that are organized and stabilized by membrane proteins, such as cholesterol, which interacts with NrCAM through its palmitoylated residues (Ren and Bennett, 1998), could also contribute to the restriction of diffusion. Another probable factor is the appearance of a specific brevican-containing extracellular matrix that ensheathes the AIS in mature neurons (Hedstrom et al., 2007) and is likely to affect diffusion of membrane proteins (Frischknecht et al., 2009).

Physiological role of the modulation of protein mobility at the AIS

This major role of a scaffolding protein in restricting membrane protein diffusion and ultimately localization is reminiscent of what has been consistently found at the postsynaptic compartment. Direct or indirect interactions of neurotransmitter receptors with scaffolds drive receptor concentration and play a role in modulating their presence at the synapse. At excitatory synapses, AMPA receptors associate with stargazin, resulting in the immobilization of AMPA–stargazin complexes (Bats et al., 2007). At inhibitory synapses, γ-aminobutyric acid and glycine receptors bind to gephyrin, which leads to their concentration at the postsynaptic density (Renner et al., 2008). Furthermore, modulation of receptor concentration at synapses by neuronal activity could occur through regulation of the scaffold–receptor binding strength, suggesting a mechanism for synaptic plasticity (Ehrensperger et al., 2007; Newpher and Ehlers, 2008). Here, we clearly show that Kv-Nav diffusion at the AIS is linked to its capability to bind ankG, demonstrating that a regulation of scaffold–membrane protein interaction can drive differences in diffusional behavior. It must be noted that such a regulation implies that the scaffold is in excess relative to the membrane protein, which seems to be the case for ankG at the AIS (Davis and Bennett, 1984). In addition, the modulation of ankG binding to Kv-Nav is caused by phosphorylation by a specific kinase (CK2; Bréchet et al., 2008), and we were able to detect the regulatory role of CK2 on Kv-Nav diffusion in young neurons. As the AIS has recently been shown to be modulated by neuronal activity (Grubb and Burrone, 2010a; Kuba et al., 2010), it would be very interesting to test whether variation in Nav1 diffusive properties, as well as its dynamic regulation by CK2 phosphorylation, play a role in this new mechanism of neuronal intrinsic plasticity.

Materials and methods

DNA constructs
The myc–Kv2.1-Nav1.2 1,080–1,203 (Kv-Nav) chimera and point mutant constructs have been described previously (Bréchet et al., 2008). HA–Kv2.1-Nav1.2 1,080–1,203-GFP (GFP–Kv-Nav) was generated from myc–Kv2.1-Nav1.2 1,080–1,203. The ApaI–ApaI fragment of this construct was introduced into the ApaI sites of plasmid containing EGFP–Kv2.1 (HA; gift of M.M. Tamkun, Colorado State University, Ft. Collins, CO). GFP–Kv-Nav mutants were obtained by sequential PCR amplification using a site-directed mutagenesis kit (QuickChange XL; Agilent Technologies).

NrCAM-GFP plasmid, in which the FNIII domains were replaced by the GFP, was provided by C. Faivre-Sarrailh (Centre National de la Recherche Scientifique, Marseille, France; Falk et al., 2004). To obtain NrCAM-mCherry, GFP was substituted for mCherry into AgeI–XhoI sites. 270 kD ankG-GFP plasmid was a donation from V. Bennett (Duke University Medical Center, Durham, NC). All of the generated constructs were verified by DNA sequencing.

Cell culture and transfection
Neuroblastoma cell line N2As were cultured in DME–GlutaMAX medium (Invitrogen) supplemented with 10% fetal calf serum (ABCyS), nonessential amino acids, and sodium pyruvate (Invitrogen). Transfection was performed using jetPEI (Polyplus Transfection). Transfected N2A cells were then cultured in serum-free medium (Opti-MEM–GlutaMAX; Invitrogen) to induce differentiation overnight.

Primary hippocampal neurons were prepared as previously described (Goslin and Banker, 1989; Garrido et al., 2003). Neurons were transfected at DIV 3 or DIV 8–9 using Lipofectamine 2000 (Invitrogen) according to the manufacturer's instructions. Experiments were performed 18–25 h after transfection.

Kv-Nav QD-based tracking
Hippocampal neurons were cotransfected with NrCAM-GFP or ankG-GFP and Kv-Nav or Kv-Nav mutants. When transfected in neurons, NrCAM-GFP and ankG-GFP were concentrated at the AIS, and thus GFP fluorescence concentration was used to localize the AIS in living cells. Conversely, proximal neurites not exhibiting GFP concentration were considered as proximal dendrites.

Neurons were incubated for 10 min at room temperature with 1 µg/ml rabbit polyclonal anti-myc (Abcam). Cells were then washed in neurobasal medium (Invitrogen) and incubated for 2 min at room temperature with 605 nm QDs conjugated to 0.1–1 nm F(ab')2 anti-rabbit (Invitrogen). QDs were previously incubated with 1% casein to block nonspecific binding. After three fast rinses, coverslips were mounted in a sealed custom chamber filled with imaging buffer (120 mM NaCl, 3 mM KCl, 2 mM CaCl$_2$, 2 mM MgCl$_2$, 10 mM glucose, 10 mM Hepes, pH 7.35, and 250 mOsm). Neurons were imaged at 37°C on an inverted microscope (Axiovert 200; Carl Zeiss, Inc.) equipped with a 63× oil immersion objective (NA = 1.4) and illuminated by a halogen lamp (HBO 100; OSRAM GmbH). GFP and QDs were detected using appropriate excitation and emission filters (band pass (bp) 475/40–bp 530/50 for GFP signal and bp 546/12–long pass 590 for QD signal). 512 consecutive frames were acquired at 13.3 Hz with a charge-coupled device (CCD) camera (Cool-Snap HQ; Photometrics). All recordings were done within 30 min after mounting the chamber.

N2A cells were cotransfected with GFP or ankG-GFP and Kv-Nav or Kv-Nav mutants. Cells were treated and imaged in the same conditions as neurons with the exception that N2A cells were washed in PBS and imaged in MEM medium (Invitrogen) supplemented with 20 mM Hepes.

Trajectory analysis
QDs were detected and tracked using multidimensional image analysis software (Racine et al., 2006) run by MetaMorph (MDS Analytical Technologies) with subsequent reconnection performed with routines written in Matlab (MathWorks). QDs exhibit a discontinuous fluorescence emission with "off" periods (blinking), allowing us to unambiguously detect single QDs. Trajectories were reconnected during off periods using the Matlab routines, adapting for each video the maximum duration of the fluorescence disappearance and the maximum distance covered by the QDs during off periods. For N2A experiments, parameters for the reconnection of the trajectories during off periods were kept constant among videos. The MSD was calculated using MSD (ndt) = $(N - n)^{-1}\sum_{i\,=\,1}^{N-n}((x_{i+n} - x_i)^2 + ((y_{i+n} - y_i)^2)dt$, where x_i and y_i are the coordinates of the tracked object on frame i, N is the total number of steps in the trajectory, and dt is the time interval between two successive frames. Instantaneous diffusion coefficients were calculated from linear fits of the $n = 1–8$ values of the MSD using MSD(t) = 4 Dt.

Inhibition of CK2 activity

Inhibition of CK2 activity was performed using the CK2 inhibitor DMAT (Pagano et al., 2004). DMAT (EMD) was dissolved in DMSO at 10 mM. For long-term treatment experiments, DMAT was added to the culture medium at a final concentration of 50 µM. Corresponding amounts of DMSO (vehicle) were added to the medium of control cells.

For DMAT acute application experiments, coverslips were first mounted in an open chamber (Life Imaging Services) with imaging buffer, transfected neurons were chosen, and control QD trajectories were recorded. Then, the imaging buffer was replaced by the same medium supplemented with 50 µM DMAT or DMSO as a vehicle, and the same QDs were then imaged every 5 min for 20–25 min. Imaging was performed as described in the previous section with the exception that GFP and QDs were detected using different excitation and emission filters (bp 470/40–bp 525/50 for GFP signal and bp 525/45–bp 605/20 for QD signal). 1,024 consecutive frames were acquired at 27 Hz with a CCD camera (QuantEM:512SC; Photometrics). Only QDs that were initially immobile ($D \leq 0.00075$ µm^2.s^{-1} before application of DMAT) were considered for the analysis of immobilization inhibition by DMAT.

FRAP experiments

Experiments were conducted on a wide-field FRAP imaging system (L5D; Institut Curie/Roper Industries) run by MetaMorph software using routines developed at the imaging platform of the Curie Institute. The microscope (DM6000; Leica) was equipped with a 63× objective, a monochromator for wide-field fluorescence excitation (Cairn Research), and an emission filter wheel (Sutter Instrument Co.).

Hippocampal neurons were cotransfected with NrCAM-mCherry and GFP–Kv-Nav or mutated GFP–Kv-Nav. The AIS of transfected neurons was visualized by NrCAM-mCherry fluorescence concentration. Conversely, proximal neurites not exhibiting NrCAM-mCherry concentration were considered as proximal dendrites. For FRAP experiments, only the GFP channel was recorded. Cells were mounted in a custom sealed recording chamber in imaging medium (145 mM NaCl, 5 mM KCl, 2 mM CaCl$_2$, 1 mM MgCl$_2$, 10 mM glucose, 10 mM Hepes, 0.2% BSA, pH 7.39, and 280 mOsm) and maintained at 37°C. One to three circular regions (Gaussian profile beam of 1-µm width) on each AIS were bleached by high-intensity illumination using a 200-mW solid state 488-nm Sapphire laser (Coherent, Inc.) for 15 ms at 15 mW, reducing local fluorescence by 50–80%. Recovery was monitored by time-lapse acquisitions (one frame every second for 180 s) with a back-illuminated CCD (Cascade II; Photometrics). Illumination intensity was set to prevent observational photobleaching (<10% in 200 frames). Fluorescence intensities were preliminarily corrected for background signal. Fluorescence signal was then normalized and corrected for ongoing photobleaching with the following equation: Fcorrt = (Ft/F0)/(Fnbt/Fnb0), where Ft is the fluorescence at time t, F0 is the fluorescence before bleaching, Fnbt is the mean fluorescence intensity of whole nonbleached image at time t, and Fnb0 is the mean fluorescence intensity of the whole nonbleached image before bleaching (Phair et al., 2003). Best fits of FRAP recovery curves were made according to the following equation: F(t) = Fmax(1 − exp(−Kt)), where Fmax is the normalized maximal fluorescence limit for an infinite recovery time, and K is the inverse recovery time constant. Half-time recovery is defined as 0.6932/K.

Immunocytochemistry

For immunohistochemistry, cells were fixed with 4% paraformaldehyde for 20 min at room temperature. Nonspecific binding was blocked with 0.22% gelatin in 0.1 M phosphate buffer for 30 min. For labeling of transfected Kv-Nav and mutants, cells were incubated for 1 h with mouse monoclonal antibody to myc (1:200; Roche). Endogenous proteins (ankG, Nav1, NF-186, and microtubule-associated protein 2 [MAP2]) were then immunodetected after a permeabilization step (1-min incubation in 10% Triton X-100 for Nav1 labeling or 0.066% saponin and 0.22% gelatin in phosphate buffer) with rabbit polyclonal antibody to ankG (1:400–1,000; a gift from G. Alcaraz, Institut National de la Santé et de la Recherche Médicale, Marseille, France), mouse antibody to sodium channel (panNav; 1:100; Sigma-Aldrich), rabbit polyclonal antibody to NF-186 (1:200; a gift from V. Bennett), and chicken polyclonal antibody to MAP2 (1:10,000; Abcam). Corresponding secondary antibodies conjugated to Alexa Fluor 488, 546, and 633 were incubated for 45 min (dilution from 1:400 to 1:800; Invitrogen). Coverslips were mounted in Fluor Save reagent (EMD).

Confocal microscopy and quantification

Cells were imaged using a confocal microscope (TCS-SPE or TSC-SP2; LCS or LAS-AF software; Leica). Confocal images were acquired with 40×/1.25 NA and 63×/1.40 NA oil objectives (Leica) at ambient temperature.

Fluorescence was collected as Z stacks with sequential wavelength acquisition. Quantification was performed using ImageJ software (National Institutes of Health). Regions of interest corresponding to AIS were manually selected on ankG and/or Nav1 images and reported on other channels for intensity measurements. All intensities were corrected for background labeling. For illustration, image editing was performed using ImageJ or Photoshop CS4 (Adobe) and was limited to rolling-ball background subtraction, linear-contrast enhancement, and γ adjustment.

Statistical analysis

Statistical analyses were performed with Prism software (GraphPad Software, Inc.). The parametric two-tailed *t* test was used for steady-state localization experiments, and the nonparametric tests (MW, WSR, and KS) were applied for diffusion experiments given to the anomalous nature of data distributions. Comparison of DIDC was performed using a KS.

Online supplemental material

Fig. S1 demonstrates that accumulation of endogenous ankG is sufficient to account for the reduction of Kv-Nav mobility in young neurons. Fig. S2 shows that overexpression of ankG is not sufficient to induce a diffusion barrier in young neurons. Online supplemental material is available at http://www.jcb.org/cgi/content/full/jcb.201003042/DC1.

References

Angelides, K.J., L.W. Elmer, D. Loftus, and E. Elson. 1988. Distribution and lateral mobility of voltage-dependent sodium channels in neurons. *J. Cell Biol.* 106:1911–1925. doi:10.1083/jcb.106.6.1911

Bats, C., L. Groc, and D. Choquet. 2007. The interaction between Stargazin and PSD-95 regulates AMPA receptor surface trafficking. *Neuron.* 53:719–734. doi:10.1016/j.neuron.2007.01.030

Berghs, S., D. Aggujaro, R. Dirkx Jr., E. Maksimova, P. Stabach, J.M. Hermel, J.P. Zhang, W. Philbrick, V. Slepnev, T. Ort, and M. Solimena. 2000. βIV spectrin, a new spectrin localized at axon initial segments and nodes of ranvier in the central and peripheral nervous system. *J. Cell Biol.* 151:985–1002. doi:10.1083/jcb.151.5.985

Boiko, T., M. Vakulenko, H. Ewers, C.C. Yap, C. Norden, and B. Winckler. 2007. Ankyrin-dependent and -independent mechanisms orchestrate axonal compartmentalization of L1 family members neurofascin and L1/neuron-glia cell adhesion molecule. *J. Neurosci.* 27:590–603. doi:10.1523/JNEUROSCI.4302-06.2007

Borgdorff, A.J., and D. Choquet. 2002. Regulation of AMPA receptor lateral movements. *Nature.* 417:649–653. doi:10.1038/nature00780

Bréchet, A., M.P. Fache, A. Brachet, G. Ferracci, A. Baude, M. Irondelle, S. Pereira, C. Leterrier, and B. Dargent. 2008. Protein kinase CK2 contributes to the organization of sodium channels in axonal membranes by regulating their interactions with ankyrin G. *J. Cell Biol.* 183:1101–1114. doi:10.1083/jcb.200805169

Burack, M.A., M.A. Silverman, and G. Banker. 2000. The role of selective transport in neuronal protein sorting. *Neuron.* 26:465–472. doi:10.1016/S0896-6273(00)81178-2

Chung, H.J., Y.N. Jan, and L.Y. Jan. 2006. Polarized axonal surface expression of neuronal KCNQ channels is mediated by multiple signals in the KCNQ2 and KCNQ3 C-terminal domains. *Proc. Natl. Acad. Sci. USA.* 103:8870–8875. doi:10.1073/pnas.0603376103

Clark, B.D., E.M. Goldberg, and B. Rudy. 2009. Electrogenic tuning of the axon initial segment. *Neuroscientist*. 15:651–668. doi:10.1177/1073858409341973

Dahan, M., S. Lévi, C. Luccardini, P. Rostaing, B. Riveau, and A. Triller. 2003. Diffusion dynamics of glycine receptors revealed by single-quantum dot tracking. *Science*. 302:442–445. doi:10.1126/science.1088525

Davis, J.Q., and V. Bennett. 1984. Brain ankyrin. Purification of a 72,000 Mr spectrin-binding domain. *J. Biol. Chem.* 259:1874–1881.

Davis, J.Q., S. Lambert, and V. Bennett. 1996. Molecular composition of the node of Ranvier: identification of ankyrin-binding cell adhesion molecules neurofascin (mucin+/third FNIII domain-) and NrCAM at nodal axon segments. *J. Cell Biol.* 135:1355–1367. doi:10.1083/jcb.135.5.1355

Dzhashiashvili, Y., Y. Zhang, J. Galinska, I. Lam, M. Grumet, and J.L. Salzer. 2007. Nodes of Ranvier and axon initial segments are ankyrin G-dependent domains that assemble by distinct mechanisms. *J. Cell Biol.* 177:857–870. doi:10.1083/jcb.200612012

Ehrensperger, M.V., C. Hanus, C. Vannier, A. Triller, and M. Dahan. 2007. Multiple association states between glycine receptors and gephyrin identified by SPT analysis. *Biophys. J.* 92:3706–3718. doi:10.1529/biophysj.106.095596

Fache, M.P., A. Moussif, F. Fernandes, P. Giraud, J.J. Garrido, and B. Dargent. 2004. Endocytotic elimination and domain-selective tethering constitute a potential mechanism of protein segregation at the axonal initial segment. *J. Cell Biol.* 166:571–578. doi:10.1083/jcb.200312155

Falk, J., O. Thoumine, C. Dequidt, D. Choquet, and C. Faivre-Sarrailh. 2004. NrCAM coupling to the cytoskeleton depends on multiple protein domains and partitioning into lipid rafts. *Mol. Biol. Cell.* 15:4695–4709. doi:10.1091/mbc.E04-03-0171

Frischknecht, R., M. Heine, D. Perrais, C.I. Seidenbecher, D. Choquet, and E.D. Gundelfinger. 2009. Brain extracellular matrix affects AMPA receptor lateral mobility and short-term synaptic plasticity. *Nat. Neurosci.* 12:897–904. doi:10.1038/nn.2338

Garrido, J.J., P. Giraud, E. Carlier, F. Fernandes, A. Moussif, M.P. Fache, D. Debanne, and B. Dargent. 2003. A targeting motif involved in sodium channel clustering at the axonal initial segment. *Science.* 300:2091–2094. doi:10.1126/science.1085167

Garver, T.D., Q. Ren, S. Tuvia, and V. Bennett. 1997. Tyrosine phosphorylation at a site highly conserved in the L1 family of cell adhesion molecules abolishes ankyrin binding and increases lateral mobility of neurofascin. *J. Cell Biol.* 137:703–714. doi:10.1083/jcb.137.3.703

Gil, O.D., T. Sakurai, A.E. Bradley, M.Y. Fink, M.R. Cassella, J.A. Kuo, and D.P. Felsenfeld. 2003. Ankyrin binding mediates L1CAM interactions with static components of the cytoskeleton and inhibits retrograde movement of L1CAM on the cell surface. *J. Cell Biol.* 162:719–730. doi:10.1083/jcb.200211011

Goslin, K., and G. Banker. 1989. Experimental observations on the development of polarity by hippocampal neurons in culture. *J. Cell Biol.* 108:1507–1516. doi:10.1083/jcb.108.4.1507

Groc, L., and D. Choquet. 2008. Measurement and characteristics of neurotransmitter receptor surface trafficking (Review). *Mol. Membr. Biol.* 25:344–352. doi:10.1080/09687680801958364

Grubb, M.S., and J. Burrone. 2010a. Activity-dependent relocation of the axon initial segment fine-tunes neuronal excitability. *Nature.* 465:1070–1074. doi:10.1038/nature09160

Grubb, M.S., and J. Burrone. 2010b. Building and maintaining the axon initial segment. *Curr. Opin. Neurobiol.* 20:481–488.

Hedstrom, K.L., X. Xu, Y. Ogawa, R. Frischknecht, C.I. Seidenbecher, P. Shrager, and M.N. Rasband. 2007. Neurofascin assembles a specialized extracellular matrix at the axon initial segment. *J. Cell Biol.* 178:875–886. doi:10.1083/jcb.200705119

Hedstrom, K.L., Y. Ogawa, and M.N. Rasband. 2008. AnkyrinG is required for maintenance of the axon initial segment and neuronal polarity. *J. Cell Biol.* 183:635–640. doi:10.1083/jcb.200806112

Holcman, D., and A. Triller. 2006. Modeling synaptic dynamics driven by receptor lateral diffusion. *Biophys. J.* 91:2405–2415. doi:10.1529/biophysj.106.081935

Inda, M.C., J. DeFelipe, and A. Muñoz. 2006. Voltage-gated ion channels in the axon initial segment of human cortical pyramidal cells and their relationship with chandelier cells. *Proc. Natl. Acad. Sci. USA.* 103:2920–2925. doi:10.1073/pnas.0511197103

Kobayashi, T., B. Storrie, K. Simons, and C.G. Dotti. 1992. A functional barrier to movement of lipids in polarized neurons. *Nature.* 359:647–650. doi:10.1038/359647a0

Kordeli, E., S. Lambert, and V. Bennett. 1995. AnkyrinG. A new ankyrin gene with neural-specific isoforms localized at the axonal initial segment and node of Ranvier. *J. Biol. Chem.* 270:2352–2359. doi:10.1074/jbc.270.5.2352

Kuba, H., Y. Oichi, and H. Ohmori. 2010. Presynaptic activity regulates Na(+) channel distribution at the axon initial segment. *Nature.* 465:1075–1078. doi:10.1038/nature09087

Lasiecka, Z.M., C.C. Yap, M. Vakulenko, and B. Winckler. 2008. Compartmentalizing the neuronal plasma membrane from axon initial segments to synapses. *Int. Rev. Cell Mol. Biol.* 272:303–389. doi:10.1016/S1937-6448(08)01607-9

Lemaillet, G., B. Walker, and S. Lambert. 2003. Identification of a conserved ankyrin-binding motif in the family of sodium channel alpha subunits. *J. Biol. Chem.* 278:27333–27339. doi:10.1074/jbc.M303327200

Li, M., Y.N. Jan, and L.Y. Jan. 1992. Specification of subunit assembly by the hydrophilic amino-terminal domain of the Shaker potassium channel. *Science.* 257:1225–1230. doi:10.1126/science.1519059

Lim, S.T., D.E. Antonucci, R.H. Scannevin, and J.S. Trimmer. 2000. A novel targeting signal for proximal clustering of the Kv2.1 K+ channel in hippocampal neurons. *Neuron.* 25:385–397. doi:10.1016/S0896-6273(00)80902-2

Lorincz, A., and Z. Nusser. 2008. Cell-type-dependent molecular composition of the axon initial segment. *J. Neurosci.* 28:14329–14340. doi:10.1523/JNEUROSCI.4833-08.2008

Martin, P.M., M. Carnaud, G. Garcia del Caño, M. Irondelle, T. Irinopoulou, J.A. Girault, B. Dargent, and L. Goutebroze. 2008. Schwannomin-interacting protein-1 isoform IQCJ-SCHIP-1 is a late component of nodes of Ranvier and axon initial segments. *J. Neurosci.* 28:6111–6117. doi:10.1523/JNEUROSCI.1044-08.2008

Nakada, C., K. Ritchie, Y. Oba, M. Nakamura, Y. Hotta, R. Iino, R.S. Kasai, K. Yamaguchi, T. Fujiwara, and A. Kusumi. 2003. Accumulation of anchored proteins forms membrane diffusion barriers during neuronal polarization. *Nat. Cell Biol.* 5:626–632. doi:10.1038/ncb1009

Newpher, T.M., and M.D. Ehlers. 2008. Glutamate receptor dynamics in dendritic microdomains. *Neuron.* 58:472–497. doi:10.1016/j.neuron.2008.04.030

Nishimura, K., H. Akiyama, M. Komada, and H. Kamiguchi. 2007. betaIV-spectrin forms a diffusion barrier against L1CAM at the axon initial segment. *Mol. Cell. Neurosci.* 34:422–430. doi:10.1016/j.mcn.2006.11.017

Ogawa, Y., and M.N. Rasband. 2008. The functional organization and assembly of the axon initial segment. *Curr. Opin. Neurobiol.* 18:307–313. doi:10.1016/j.conb.2008.08.008

Pagano, M.A., F. Meggio, M. Ruzzene, M. Andrzejewska, Z. Kazimierczuk, and L.A. Pinna. 2004. 2-Dimethylamino-4,5,6,7-tetrabromo-1H-benzimidazole: a novel powerful and selective inhibitor of protein kinase CK2. *Biochem. Biophys. Res. Commun.* 321:1040–1044. doi:10.1016/j.bbrc.2004.07.067

Pan, Z., T. Kao, Z. Horvath, J. Lemos, J.Y. Sul, S.D. Cranstoun, V. Bennett, S.S. Scherer, and E.C. Cooper. 2006. A common ankyrin-G-based mechanism retains KCNQ and NaV channels at electrically active domains of the axon. *J. Neurosci.* 26:2599–2613. doi:10.1523/JNEUROSCI.4314-05.2006

Phair, R.D., S.A. Gorski, and T. Misteli. 2003. Measurement of dynamic protein binding to chromatin in vivo, using photobleaching microscopy. *Methods Enzymol.* 375:393–414. doi:10.1016/S0076-6879(03)75025-3

Racine, V., A. Hertzog, J. Jouanneau, J. Salamero, C. Kervrann, and J.-B. Sibarita. 2006. Multiple-target tracking of 3D fluorescent objects based on simulated annealing. Third IEEE International Symposium on Biomedical Imaging. 1020–1023. doi:10.1109/ISBI.2006.1625094

Rasmussen, H.B., C. Frøkjaer-Jensen, C.S. Jensen, H.S. Jensen, N.K. Jørgensen, H. Misonou, J.S. Trimmer, S.P. Olesen, and N. Schmitt. 2007. Requirement of subunit co-assembly and ankyrin-G for M-channel localization at the axon initial segment. *J. Cell Sci.* 120:953–963. doi:10.1242/jcs.03396

Ren, Q., and V. Bennett. 1998. Palmitoylation of neurofascin at a site in the membrane-spanning domain highly conserved among the L1 family of cell adhesion molecules. *J. Neurochem.* 70:1839–1849. doi:10.1046/j.1471-4159.1998.70051839.x

Renner, M., C.G. Specht, and A. Triller. 2008. Molecular dynamics of postsynaptic receptors and scaffold proteins. *Curr. Opin. Neurobiol.* 18:532–540. doi:10.1016/j.conb.2008.09.009

Salzer, J.L. 2003. Polarized domains of myelinated axons. *Neuron.* 40:297–318. doi:10.1016/S0896-6273(03)00628-7

Sekimoto, K., and A. Triller. 2009. Compatibility between itinerant synaptic receptors and stable postsynaptic structure. *Phys. Rev. E Stat. Nonlin. Soft Matter Phys.* 79:031905.

Sobotzik, J.M., J.M. Sie, C. Politi, D. Del Turco, V. Bennett, T. Deller, and C. Schultz. 2009. AnkyrinG is required to maintain axo-dendritic polarity in vivo. *Proc. Natl. Acad. Sci. USA.* 106:17564–17569. doi:10.1073/pnas.0909267106

Song, A.H., D. Wang, G. Chen, Y. Li, J. Luo, S. Duan, and M.M. Poo. 2009. A selective filter for cytoplasmic transport at the axon initial segment. *Cell.* 136:1148–1160. doi:10.1016/j.cell.2009.01.016

Specht, C.G., and A. Triller. 2008. The dynamics of synaptic scaffolds. *Bioessays.* 30:1062–1074. doi:10.1002/bies.20831

Srinivasan, Y., L. Elmer, J. Davis, V. Bennett, and K. Angelides. 1988. Ankyrin and spectrin associate with voltage-dependent sodium channels in brain. *Nature.* 333:177–180. doi:10.1038/333177a0

Tardin, C., L. Cognet, C. Bats, B. Lounis, and D. Choquet. 2003. Direct imaging of lateral movements of AMPA receptors inside synapses. *EMBO J.* 22:4656–4665. doi:10.1093/emboj/cdg463

Triller, A., and D. Choquet. 2008. New concepts in synaptic biology derived from single-molecule imaging. *Neuron.* 59:359–374. doi:10.1016/j.neuron.2008.06.022

Winckler, B., P. Forscher, and I. Mellman. 1999. A diffusion barrier maintains distribution of membrane proteins in polarized neurons. *Nature.* 397:698–701. doi:10.1038/17806

Xu, X., and P. Shrager. 2005. Dependence of axon initial segment formation on Na+ channel expression. *J. Neurosci. Res.* 79:428–441. doi:10.1002/jnr.20378

Yang, Y., Y. Ogawa, K.L. Hedstrom, and M.N. Rasband. 2007. βIV spectrin is recruited to axon initial segments and nodes of Ranvier by ankyrinG. *J. Cell Biol.* 176:509–519. doi:10.1083/jcb.200610128

Zhou, D., S. Lambert, P.L. Malen, S. Carpenter, L.M. Boland, and V. Bennett. 1998. Ankyrin$_G$ is required for clustering of voltage-gated Na channels at axon initial segments and for normal action potential firing. *J. Cell Biol.* 143:1295–1304. doi:10.1083/jcb.143.5.1295